Available online at www.sciencedirect.com
SCIENCE DIRECT®
International Journal of Heat and Fluid Flow 24 (2003) 463–469
International Journal of HEAT AND FLUID FLOW
www.elsevier.com/locate/ijhff

Numerical simulation of the flow around a circular cylinder at high Reynolds numbers

Pietro Catalano [a,*], Meng Wang [b], Gianluca Iaccarino [b], Parviz Moin [b]

[a] CIRA—Italian Aerospace Research Center, 81043 Capua (CE), Italy
[b] Center for Turbulence Research, Stanford University/NASA Ames Research Center, Stanford, CA 94305-3030, USA

Received 30 November 2002; accepted 23 March 2003

Abstract

The viability and accuracy of large-eddy simulation (LES) with wall modeling for high Reynolds number complex turbulent flows is investigated by considering the flow around a circular cylinder in the supercritical regime. A simple wall stress model is employed to provide approximate boundary conditions to the LES. The results are compared with those obtained from steady and unsteady Reynolds-averaged Navier–Stokes (RANS) solutions and the available experimental data. The LES solutions are shown to be considerably more accurate than the RANS results. They capture correctly the delayed boundary layer separation and reduced drag coefficients consistent with experimental measurements after the drag crisis. The mean pressure distribution is predicted reasonably well at $Re_D = 5 \times 10^5$ and 10^6. However, the Reynolds number dependence is not captured, and the solution becomes less accurate at increased Reynolds numbers.

Keywords: Large-eddy simulation; Wall modeling; Unsteady RANS; High Reynolds number flows; Circular cylinder; Navier–Stokes equations

1. Introduction

The severe grid-resolution requirement in the near-wall region has been the major roadblock to the use of large-eddy simulation (LES) for practical applications. This arises because of the presence of small but dynamically important eddies in the near-wall region. To resolve these vortical structures, the number of grid points required scales as the square of the friction Reynolds number (Baggett et al., 1997), which is nearly the same as for direct numerical simulation.

As a practical remedy, LES can be combined with a wall-layer model. In this approach, LES is conducted on a relatively coarse mesh which scales with the outer flow scale, thus making the computational cost only weakly dependent on the Reynolds number. The dynamic effects of energy-containing eddies in the wall layer (viscous and buffer regions) are determined from a wall model which provides to the outer LES a set of approximate boundary conditions, often in the form of wall shear stresses.

In recent years, wall models based on turbulent boundary layer (TBL) equations and their simplified forms have received much attention. These models, used with a Reynolds-averaged Navier–Stokes (RANS) type eddy viscosity, have shown good promise. The approach has been successfully tested by Balaras et al. (1996) in a plane channel, square duct, and rotating channel, and by Cabot and Moin (2000) in a plane channel and backward-facing step. More recently, Wang and Moin (2002) employed this approach to simulate the flow past the trailing-edge of an airfoil at chord Reynolds number of 2.15×10^6, and obtained very good agreement with solutions from the full LES (Wang and Moin, 2000) at a small fraction of the computational cost.

The main objectives of the present work are to further assess the viability and accuracy of LES with wall modeling for high Reynolds number complex turbulent flows and to compare this approach with RANS models. To this end, the flow around a circular cylinder at Reynolds numbers (based on the cylinder diameter D)

* Corresponding author. Tel.: +39-0823-623244; fax: +39-0823-623-028.
E-mail address: p.catalano@cira.it (P. Catalano).

0142-727X/03/$ - see front matter © 2003 Elsevier Science Inc. All rights reserved.
doi:10.1016/S0142-727X(03)00061-4

of 0.5×10^6, 1×10^6 and 2×10^6 is considered, and the results are compared to those from steady and unsteady RANS and the available experimental data. The flow around a circular cylinder, with its complex features, represents a canonical problem for validating new approaches in computational fluid dynamics. To take the best advantage of wall modeling, we have concentrated on the super-critical flow regime in which the boundary layer becomes turbulent prior to separation. This is, to the authors' knowledge, the first such attempt using LES. A related method, known as detached eddy simulation (DES), in which the entire attached boundary layer is modeled, has been tested for this type of flow by Travin et al. (1999). Recently an LES study has been conducted by Breuer (2000) at a high sub-critical Reynolds number of 1.4×10^5, and a good comparison with the experimental data, especially in the near wake, has been shown.

2. Numerical method for LES

The numerical method for LES and wall model implementation are the same as in Wang and Moin (2002). The energy-conservative scheme, written in a staggered grid system in body-fitted coordinates, is of hybrid finite difference/spectral type (Mittal and Moin, 1997); it employs second-order central differences in streamwise and wall-normal directions and Fourier collocation in the spanwise direction. The fractional step approach, in combination with the Crank–Nicholson method for viscous terms and third order Runge–Kutta scheme for the convective terms, is used for time advancement. The continuity constraint is imposed at each Runge–Kutta substep by solving a Poisson equation for pressure using a multigrid iterative procedure. The subgrid scale (SGS) stress tensor is modeled by the dynamic Smagorinsky model (Germano et al., 1991) in combination with a least-square contraction and spanwise averaging (Lilly, 1992).

Approximate boundary conditions are imposed on the cylinder surface in terms of wall shear stress components τ_{wi} ($i = 1,3$) estimated from a TBL equation-based wall model (Balaras et al., 1996; Cabot and Moin, 2000; Wang and Moin, 2002), which has the following general form in Cartesian coordinates:

$$\frac{\partial}{\partial x_2}(v + v_t)\frac{\partial u_i}{\partial x_2} = \frac{1}{\rho}\frac{\partial p}{\partial x_i} + \frac{\partial u_i}{\partial t} + \frac{\partial}{\partial x_j}u_i u_j, \quad i = 1, 3 \qquad (1)$$

where x_1, x_2, and x_3 denote the streamwise, wall-normal, and spanwise directions, respectively, and u_1, u_2 and u_3 the corresponding velocity components. Eq. (1) has been implemented in a body-fitted, locally orthogonal coordinate system as shown in Fig. 1. To make a distinction, the fixed Cartesian coordinates (see also Fig. 1) and velocities are denoted by x, y, z and u, v, w. In the present work a simplified version of the wall model is employed,

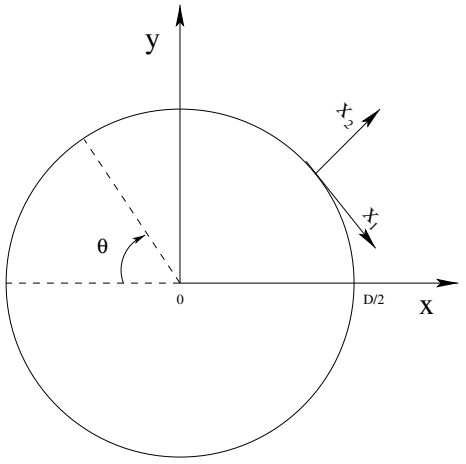

Fig. 1. Coordinate systems used. z and x_3 axes are out of the plane.

in which the substantial derivative (last two terms) is dropped from the right-hand side of Eq. (1). Since the pressure is assumed x_2-independent in the thin wall layer and is imposed from the outer flow LES solution, one can then integrate Eq. (1) to the wall to obtain a closed form expression for the wall stress components (Wang and Moin, 2002)

$$\tau_{wi} = \mu\frac{\partial u_i}{\partial x_2}\bigg|_{x_2=0} = \frac{\rho}{\int_0^\delta \frac{\mathrm{d}x_2}{\nu+\nu_t}}\left\{u_{\delta i} - \frac{1}{\rho}\frac{\partial p}{\partial x_i}\int_0^\delta \frac{\mathrm{d}x_2}{\nu+\nu_t}\,\mathrm{d}x_2\right\} \qquad (2)$$

where $u_{\delta i}$ denotes the tangential velocity components from LES at the first off-wall node, at distance δ from the wall. In attached flows these nodes are generally placed within the lower edge of the logarithmic layer. In the present flow, however, δ^+ (in wall units) is found to vary from 0 to 130 depending on the local skin friction. The eddy viscosity ν_t is obtained from a mixing length model with a near-wall damping

$$\frac{\nu_t}{\nu} = \kappa y_w^+(1 - \mathrm{e}^{-y_w^+/A})^2 \qquad (3)$$

where y_w^+ is the distance to the wall in wall units, $\kappa = 0.4$ is the von Kármán constant, and $A = 19$.

Simulations are conducted employing a C-mesh in the planes perpendicular to the span. The computational domain extends approximately $22D$ upstream of the cylinder, $17D$ downstream of the cylinder, and $24D$ into the far-field. In the streamwise direction 401 grid points, 144 of which on the cylinder surface and 2×129 points in the wake, are employed. In the wall-normal direction 120 points are used. The spanwise domain size is $2D$, over which the flow is assumed periodic, and 48 grid points are distributed uniformly. Note that the spanwise domain size is shorter than the typical values used for lower Reynolds number flows (e.g. πD for $Re_D = 3900$ in Beaudan and Moin (1994) and Kravchenko and Moin (2000)). This is justified because of the reduced spanwise

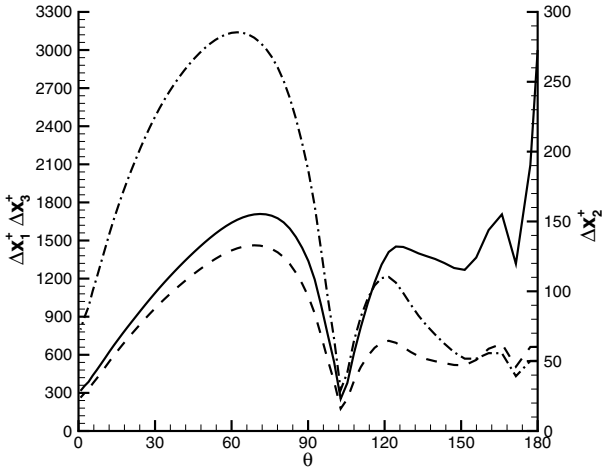

Fig. 2. Sizes of the wall-adjacent cells: (- - -) Δx_1^+; (—) Δx_2^+; (–·–) Δx_3^+.

correlation length for higher Reynolds number flows. The same spanwise domain size of $2D$ was used by Breuer (2000) at $Re_D = 1.4 \times 10^5$. Potential-flow solutions are imposed as boundary conditions in the far-field, and convective boundary conditions are used at the outflow boundary.

The sizes of the wall-adjacent grid cells for LES are shown in Fig. 2 in wall units. They are extremely large, because the use of a wall model in principle bypasses the need to resolve the inner scales. In the staggered grid system used, the first off-wall nodes for the tangential velocities are located at $\delta^+ = \Delta x_2^+/2$, where the LES and wall-model velocities are required to match. Note that the wall units in Fig. 2 are affected by the skin friction errors to be discussed later, and should thus be viewed as a crude estimate.

3. Numerical method for RANS

RANS simulations are carried out using a commercial CFD code, FLUENT. It is based on a second order finite volume discretization and the SIMPLE pressure correction technique for enforcing the divergence-free condition of the velocity field; the time integration is three-level fully implicit. The eddy viscosity is obtained using the standard k–ε model (Launder and Spalding, 1972) with wall functions. Although unstructured grids can be used in FLUENT, for the simulations presented here we employed the same C-mesh as used in the LES.

Both steady and unsteady RANS calculations have been performed for comparison. Steady simulations are performed using only half of the computational domain ($y \geqslant 0$). Starting from this solution and its mirror image in the region $y < 0$, a disturbance was imposed to break the symmetry, and a time-accurate simulation was carried out. A non-dimensional time-step $\Delta t U_\infty/D$ of 0.01 was used and the simulation was run for 300 time units (D/U_∞).

4. Results and discussion

To obtain the LES results presented here, the simulations have advanced more than 300 dimensionless time units. The statistics are collected over the last 200 time units. Running at a maximum CFL number of 1.5, the non-dimensional time step $\Delta t U_\infty/D$ typically varies between 0.0030 and 0.0045. Three Reynolds numbers, $Re_D = 0.5 \times 10^6$, 1×10^6, and 2×10^6, have been considered. The discussion will be mainly focused on the case of $Re_D = 1 \times 10^6$, with emphasis on important flow parameters, such as the drag coefficient, the base pressure coefficient, the Strouhal number, and their dependence on the Reynolds number.

The mean pressure distribution on the cylinder surface is compared to two set of experimental data in Fig. 3. A very good agreement is observed between the LES at $Re_D = 1 \times 10^6$ and the experiment by Warschauer and Leene (1971) which was performed at $Re_D = 1.2 \times 10^6$. The original data of Warschauer and Leene (1971) exhibit some spanwise variations (see Zdravkovich, 1997), and for the purpose of comparison the average values are plotted. The unsteady RANS also provides a mean pressure coefficient in satisfactory agreement with both LES and the experimental data, while, as expected, the steady RANS yields a poor result. Relative to the measurements of Falchsbart at $Re_D = 6.7 \times 10^5$, the numerical results show lower values in the base region. It is worth noting that Falchsbart's data contain a kink near $\theta = 110°$, indicating the presence of a separation bubble. This type of separation bubble is characteristic of the critical regime, and is difficult to reproduce

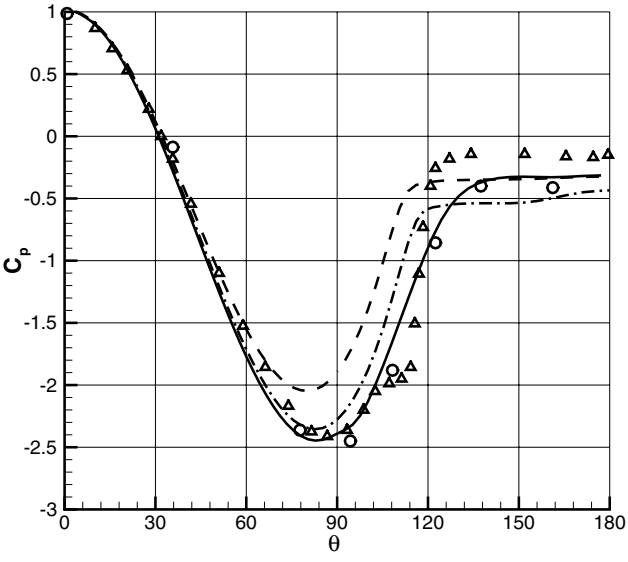

Fig. 3. Mean pressure distribution on the cylinder: (—) LES at $Re_D = 1 \times 10^6$; (- - -) RANS at $Re_D = 1 \times 10^6$; (–·–) URANS at $Re_D = 1 \times 10^6$; (○) experiment by Warschauer and Leene (1971) at $Re_D = 1.2 \times 10^6$ (spanwise averaged); (△) experiment by Falchsbart (in Zdravkovich, 1997) at $Re_D = 6.7 \times 10^5$.

experimentally or numerically due to sensitivity to disturbances.

The contours of the vorticity magnitude, as computed by LES and URANS for $Re_D = 1 \times 10^6$ at a given time instant and spanwise plane, are plotted in Fig. 4. In the LES results, some coherent structures are visible in the wake, but they are not as well organized as in typical Kármán streets at sub-critical and post-critical Reynolds numbers. The rather thick layers along the cylinder surface consist mostly of vorticity contours of small magnitude. These levels are necessary for visualizing the wake structure, but are not representative of the boundary layer thickness. The true boundary layer, with strong vorticity, is extremely thin and mostly laminar in the attached flow region. The shear layers are more coherent in the URANS than in the LES. A clear vortex-shedding pattern is exhibited in the URANS results.

The mean streamwise velocity distribution (time and spanwise averaged) obtained by LES is presented in the lower half of Fig. 5. Compared to flows at lower Reynolds numbers (Kravchenko and Moin, 2000; Breuer, 2000), the boundary layer separation is much delayed, and the wake is narrower, resulting in a smaller drag coefficient. The time-averaged URANS velocity distribution is plotted in the upper half of Fig. 5, which shows a thicker wake, resulting in a higher drag coefficient. A

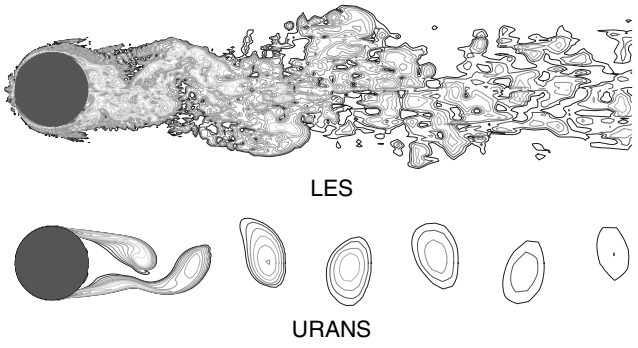

Fig. 4. Instantaneous vorticity magnitude at a given spanwise cut for flow over a circular cylinder at $Re_D = 1 \times 10^6$. 25 contour levels from $\omega D/U_\infty = 1$ to $\omega D/U_\infty = 575$ (exponential distribution) are plotted.

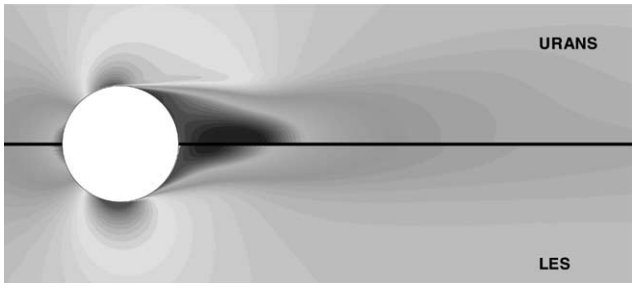

Fig. 5. Mean streamwise velocity distribution predicted by LES and URANS. 45 contour levels from $U/U_\infty = -0.2$ to $U/U_\infty = 1.7$ are plotted.

quantitative comparison between LES and URANS in terms of the mean streamwise and vertical velocity profiles in the cylinder wake is shown in Fig. 6. The upper and lower parts correspond to two streamwise locations inside and outside of the mean recirculation region, respectively. The LES predicts a wide range of flow scales and hence more mixing of the flow. The velocity deficit from LES is larger at $x/D = 0.75$, which is in the middle of the mean recirculation bubble as predicted by LES, but it is soon surpassed by the URANS prediction further downstream in the wake. Unfortunately, there is a general lack of detailed experimental data at super-critical Reynolds numbers. In particular, velocity and Reynolds-stress profile measurements are non-existent, making an experimental validation of the wake profiles impossible.

Another comparison between the LES and URANS is made in Fig. 7 in terms of lift and drag time histories. It is again clear that the URANS predicts a very well organized and periodic flow at this Reynolds number, whereas the LES results have broadband turbulence characteristics. The overly dissipative nature of the URANS calculations is also evident by observing the small amplitudes of the lift and, especially, drag oscillations.

The drag coefficient, base pressure coefficient, Strouhal number, and mean recirculation length for the flow at Reynolds number of 1×10^6 are summarized in Table 1. The agreement with the measurements of Shih et al. (1993) is reasonably good. The LES overpredicts the drag coefficient compared to Shih et al. (1993), but underpredicts the C_D relative to Achenbach (1968) (cf. Fig. 9). The Strouhal number of 0.22 from Shih et al. (1993) is for a rough cylinder. It is generally accepted that periodic vortex shedding does not exist in the super-critical regime for smooth cylinders (Shih et al., 1993; Zdravkovich, 1997). From our simulations, a distinct spectral peak is observed at $St \approx 0.35$, as shown clearly in the E_{vv} spectra in Fig. 8. This figure depicts the frequency spectra of the streamwise and vertical velocities at $x/D = 0.70$ and 1.50, $y/D = 0.15$. It can be argued that the discretization of the cylinder surface and the numerical errors due to the under-resolution may act as equivalent surface roughness, causing the flow field to acquire some rough cylinder characteristics. The wide scatter of C_D and St among various experiments in the literature (Zdravkovich, 1997), listed at the bottom of Table 1, suggests high sensitivity of the flow to perturbations due to surface roughness and free-stream turbulence in the super-critical regime. Our simulation results fall easily within the experimental range.

To assess the robustness of the computational method, LESs at $Re_D = 5 \times 10^5$ and 2×10^6 have also been performed. The predicted mean drag coefficients are plotted in Fig. 9 along with the drag curve of Achenbach (1968). The C_D at the two lower Reynolds numbers is

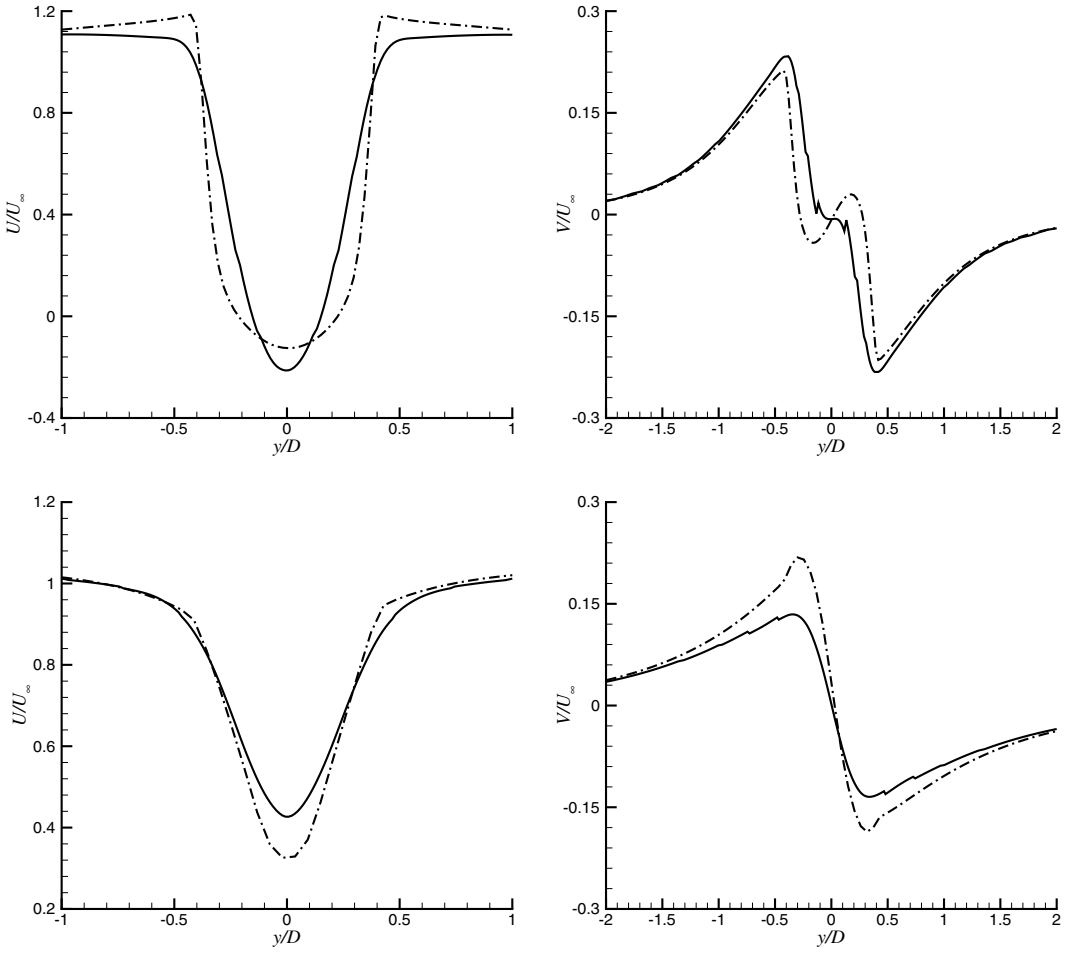

Fig. 6. Mean streamwise and vertical velocities at $x/D = 0.75$ (upper figures) and $x/D = 1.50$ (lower figures): (—) LES; (–·–) URANS.

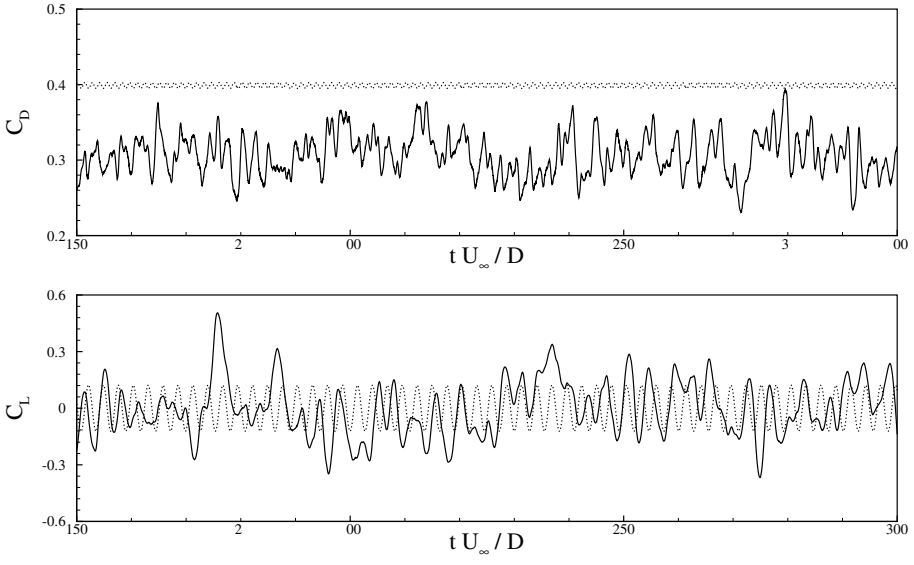

Fig. 7. Time histories of lift and drag coefficients. (—) LES; (- - -) URANS.

predicted rather well, but the discrepancy becomes large at $Re_D = 2 \times 10^6$. More significantly the LES solutions show relative insensitivity to the Reynolds number, in contrast to the experimental data that exhibit an increase in C_D after the drag crisis. Poor grid resolution, which becomes increasingly severe as the Reynolds

Table 1
Drag, base pressure coefficient, Strouhal number, and recirculation length for the flow around a circular cylinder at $Re_D = 1 \times 10^6$

	C_D	$-C_{P_{base}}$	St	L_r/D
LES	0.31	0.32	0.35	1.04
RANS	0.39	0.33	–	
URANS	0.40	0.41	0.31	1.37
Exp. (Shih et al., 1993)	0.24	0.33	0.22	–
Exp. (Others, see Zdravkovich, 1997)	0.17–0.40	–	0.18–0.50	–

number increases, is the primary suspect. Similar Reynolds number insensitivity is shown by the URANS results.

The skin friction coefficients predicted by the wall model employed in the LES computations are presented in Fig. 10 together with the experimental data of Achenbach (1968) at $Re_D = 3.6 \times 10^6$. The levels are very different on the front half of the cylinder but are in reasonable agreement on the back half. The boundary layer separation and the recirculation region are captured rather well, indicating that they are not strongly affected by the upstream errors. The different Reynolds numbers between the LES and the experiments can account for only a small fraction of the discrepancy. Note that the computed C_f values are comparable to those reported by Travin et al. (1999) using DES at $Re_D = 3 \times 10^6$. Travin et al. (1999) attribute the overprediction of the C_f before the separation to the largely laminar boundary layer that has not been adequately modeled. This is also the case in the present simulation. Both experiments and numerical simulations suggest that even at these super-critical Reynolds numbers, the boundary layers remain laminar in most of the favorable pressure gradient region. In our simulations no effort was made to trigger transition, nor was the wall model

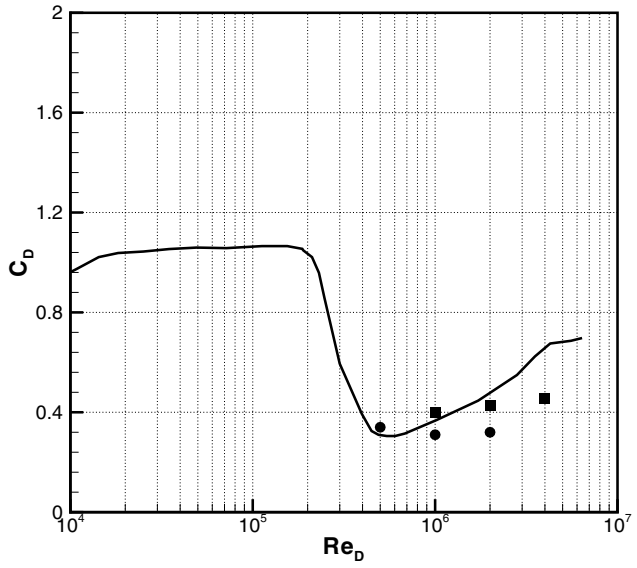

Fig. 9. Drag coefficient as a function of the Reynolds number. (—) Achenbach (1968); (●) LES; (■) URANS.

modified for laminar flow application. Grid resolution is another potential culprit in the present work. In addition, an overprediction of the skin friction by the wall model adopted in the present LES computations has also been observed by Wang and Moin (2002) in the acceleration region of the trailing-edge flow, suggesting that this simplified model may have difficulty with strong favorable pressure gradients.

5. Concluding remarks

A bold numerical experiment has been performed to compute the flow around a circular cylinder at super-

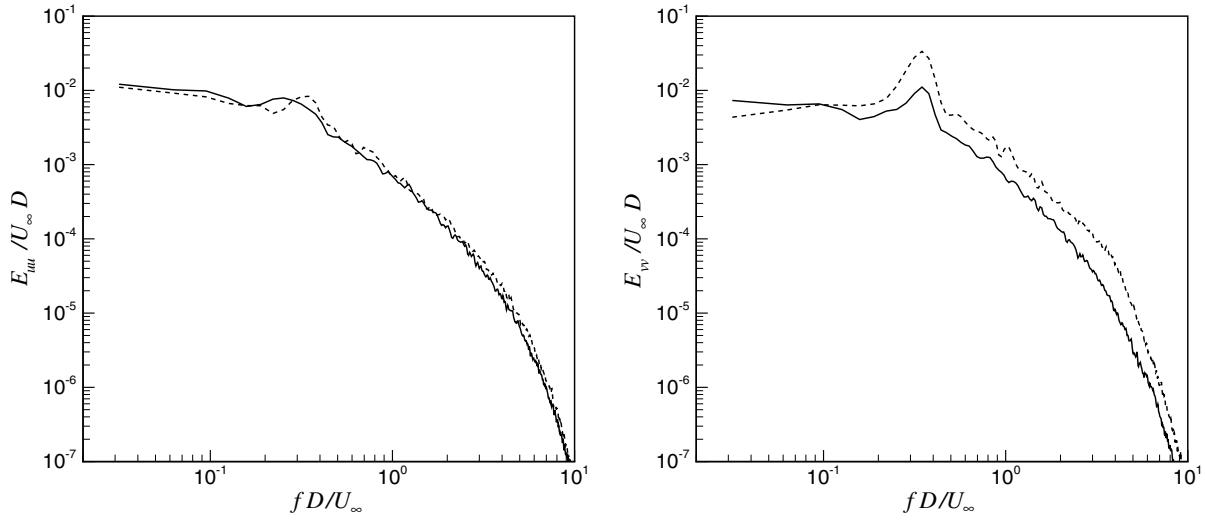

Fig. 8. Frequency spectra of streamwise (left figure) and vertical (right figure) velocities at two wake stations: (—) $x/D = 0.70$, $y/D = 0.15$; (- - -) $x/D = 1.50$, $y/D = 0.15$.

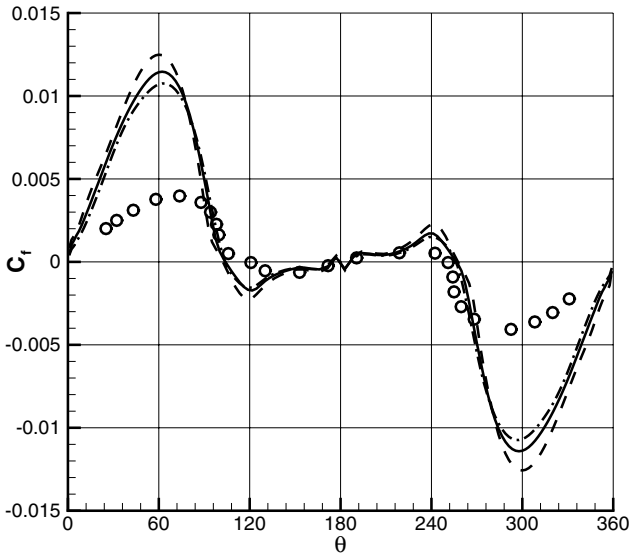

Fig. 10. Skin friction distribution on the cylinder: (- - -) LES at $Re_D = 0.5 \times 10^6$; (—) LES at $Re_D = 1 \times 10^6$; (–·–) LES at $Re_D = 2 \times 10^6$; (○) experiments by Achenbach (1968) at $Re_D = 3.62 \times 10^6$.

critical Reynolds number using LES. The simulations have been made possible by the use of a wall model that alleviates the near-wall grid resolution requirements. Preliminary results are promising in the sense that they correctly predict the delayed boundary layer separation and reduced drag coefficients consistent with measurements after the drag crisis. The mean pressure distributions and overall drag coefficients are predicted reasonably well at $Re_D = 0.5 \times 10^6$ and 1×10^6. However the computational solutions are inaccurate at higher Reynolds numbers, and the Reynolds number dependence is not captured. It should be noted that the grid used near the surface, particularly before separation, is quite coarse judged by the need to resolve the outer boundary layer scales. The effect of the wall model under coarse grid resolution and in the laminar section of the boundary layer is not clear. A more systematic investigation is needed to separate the grid resolution and the wall-modeling effects, and to fully validate the numerical methodology for this challenging flow.

Acknowledgements

This work was supported in part by the US Air Force Office of Scientific Research Grant No. F49620-00-1-0111. Computations were carried out on the NAS facilities at NASA Ames Research Center and on facilities at the Center for Turbulence Research. We would like to thank Professor Javier Jiménez for valuable discussions.

References

Achenbach, E., 1968. Distribution of local pressure and skin friction around a circular cylinder in cross-flow up to $Re = 5 \times 10^6$. J. Fluid Mech. 34, 625–639.

Baggett, J.S., Jiménez, J., Kravchenko, A.G., 1997. Resolution requirements in large eddy simulations of shear flows. Annual Research Briefs—1997. Center for Turbulence Research, Stanford University/NASA Ames, pp. 51–66.

Balaras, E., Benocci, C., Piomelli, U., 1996. Two-layer approximate boundary conditions for large eddy simulation. AIAA J. 34, 1111–1119.

Beaudan, P., Moin, P., 1994. Numerical Experiments on the Flow Past a Circular Cylinder at Subcritical Reynolds Number. Report no. TF-62, Department of Mech. Engr., Stanford University.

Breuer, M., 2000. A challenging test case for large eddy simulation: high Reynolds number circular cylinder flow. Int. J. Heat Fluid Flow 21, 648–654.

Cabot, W., Moin, P., 2000. Approximate wall boundary conditions in the large eddy simulation of high Reynolds number flow. Flow Turb. Combust. 63, 269–291.

Germano, M., Piomelli, U., Moin, P., Cabot, W.H., 1991. A dynamic subgrid-scale eddy viscosity model. Phys. fluids A 3, 1760–1765.

Kravchenko, A.G., Moin, P., 2000. Numerical studies of flow over a circular cylinder at $Re_D = 3900$. Phys. Fluids 12, 403–417.

Launder, B.E., Spalding, D.B., 1972. Mathematical Models of Turbulence. Academic Press, London.

Lilly, D.K., 1992. A proposed modification of the Germano subgrid scale closure method. Phys. Fluids A 4, 633–635.

Mittal, R., Moin, P., 1997. Suitability of upwind-biased finite difference schemes for large eddy simulation of turbulent flows. AIAA J. 35, 1415–1417.

Shih, W.C.L., Wang, C., Coles, D., Roshko, A., 1993. Experiments on flow past rough circular cylinders at large Reynolds numbers. J. Wind Eng. Indust. Aerodyn. 49, 351–368.

Travin, A., Shur, M., Strelets, M., Spalart, P., 1999. Detached eddy simulations past a circular cylinder. Flow Turb. Combust. 63, 269–291.

Wang, M., Moin, P., 2000. Computation of trailing-edge flow and noise using large-eddy simulation. AIAA J. 38 (12), 2201–2209.

Wang, M., Moin, P., 2002. Dynamic wall modeling for large-eddy simulation of complex turbulent flows. Phys. Fluids 14 (7), 2043–2051.

Warschauer, K.A., Leene, J.A., 1971. Experiments on mean and fluctuating pressures of circular cylinders at cross flow at very high Reynolds numbers. In: Proc. Int. Conf. on Wind Effects on Buildings and Structures, Tokyo, Japan (see also Zdravkovich 1997), pp. 305–315.

Zdravkovich, M.M., 1997. Flow Around Circular Cylinders. Fundamentals, vol. 1. Oxford University Press, 1997 (Chapter 6).